Quantum thermal chokelike behavior exhibited in a spin-boson model under noncommutative coupling

Xingyu Zhang ◉,* Xiufeng Cao ◉,* and Dahai He ◉†
Department of Physics and Jiujiang Research Institute, Xiamen University, Xiamen 361005, China

Studying heat transport in nonequilibrium dissipative systems is key to energy modulation. Driving thermal devices have attracted much attention from the perspective of active heat control. In this article, we explore the driving nonequilibrium spin-boson model with noncommutative coupling, which is described by a two-level system coupled to two bosonic baths in the $(x \cos\theta + z \sin\theta)$ direction and z direction (dephasing channel), respectively. Based on the noncommutativity, we propose a model with quantum thermal chokelike behavior, where the currents flowing into the two thermal baths display distinctly different oscillation amplitudes. This phenomenon leads to a transformation of a largely oscillating current from one bath to nearly nonoscillating one at the other bath. To quantify the asymmetry in the oscillation amplitudes of the currents flowing into the two baths, we introduce a thermal choke ratio. This ratio exhibits a monotonic decrease as the noncommutativity parameter vanishes. We further calculate the time-independent currents via the Floquet theory using the secular approximation and find that they coincide with the time averages of the above oscillating currents. Moreover, we investigate the dependence of these time-independent mean currents on various parameters. Our findings will advance the understanding of externally driven thermal analogs of electronic devices, and contribute to energy transport control in nanoscale systems.

I. INTRODUCTION

Controlling the thermal transport in nanosystems is a crucial problem in modern thermodynamics [1–6] with the advancement of nanotechnology. In contrast with the control of electron transport, heat is usually considered less exploitable. Over the last two decades, there have been extensive discussions about the heat conduction in the physical community. The vast majority has focused on the time-independent non-driven cases [2,7]. There has been a lot of progress concerning the study of stationary heat transport, such as thermal rectifiers [8] and negative differential thermal resistance [9,10]. These advances have enabled thermal analogs [11–15] of electronic devices, which opens new ways for precise heat management. However, research on externally driven, oscillating heat currents, which can exhibit intriguing phenomena, remains relatively unexplored [16–19]. Notably, existing studies in this area have primarily focused on the analysis of stationary mean currents, neglecting the oscillatory behavior. Consequently, the development of thermal analogs for alternating-current electronic devices remains an open frontier, both theoretically and experimentally.

One of the paradigm models for the discussions of heat conduction is the nonequilibrium spin-boson (NESB) model [8], which consists of a two-level system coupled to two bosonic baths at its two ends, i.e., boundary-driven system [20]. It has been widely explored both in the context of

quantum information and quantum thermal conduction [21–25]. Seeking for solutions of the quantum dissipative model has witnessed significant progresses both analytically and numerically. Theoretically, exact master equations [26], projection operator techniques [27], the noninteracting blip approximation [28], and polaron transformation [29–32] are usually used. Numerically, widely applied methods are the numerical renormalization group [33], quasiadiabatic propagator path integral [34,35], time-evolving matrix product operator [36], stochastic dynamical equations [37], and hierarchy equations of motion (HEOM) [38,39]. Generally, numerical approaches offer advantages in tackling complex scenarios, including strong coupling and non-Markovian regimes, while analytical methods often provide deeper physical intuition. In this work, we leverage the quantum master equation framework incorporating the polaron transformation to investigate heat currents within an externally driven NESB model. The validity of our results is further verified through comparisons with the HEOM method.

Contrary to the common NESB model [8,37], in this paper, we propose a quantum thermal chokelike model, i.e., a thermal analog of electronic chokes, which transform high-frequency alternating currents with continually changing direction into direct currents with constant direction. Specifically, the two-level system is coupled to the first bath in the $(x \cos\theta + z \sin\theta)$ direction but to the second bath in the z direction, where the former can be regarded as a generalized amplitude damping channel and the latter as a dephasing channel [40–42]. This model has attracted interests recently [43–46], but only the time-independent current has been considered so far. We find that the noncommuativity

---

*These authors contributed equally to this work.
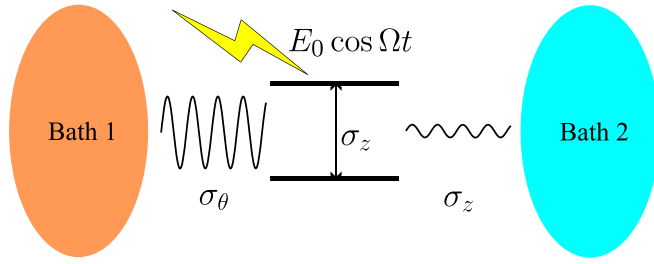†dhe@xmu.edu.cn

FIG. 1. Scheme of the model for the quantum thermal choke. The Hamiltonian of driving system is $H_S(t) = \sigma_z(E_0 \cos \Omega t + \omega_0)/2$. The first bath denotes the noncommutative coupling through $\sigma_\theta = \cos \theta \sigma_x + \sin \theta \sigma_z$, and the second bath represents the dephasing channel. The two wavy lines illustrate the asymmetry of the oscillation amplitudes of the heat currents. In this article, we utilize the natural unit $\hbar = k_B = 1$. Without specific mention, we set the energy splitting and driving parameters as $\omega_0 = 0.1\omega_c$, $E_0 = 0.3\omega_c$, $\Omega = 0.04\omega_c$, and the temperatures of two baths as $T_1 = 0.7\omega_c$, $T_2 = 0.3\omega_c$ throughout this paper.

of system-bath couplings gives rise to a distinct quantum feature in the energy transport, namely, the asymmetry of the current oscillation amplitudes. It is shown that the oscillation amplitude of the current into the second dephasing bath is largely suppressed compared to that of the first generalized amplitude damping bath. Consequently, the heat current exhibits periodic reversals of direction into the first bath, while the current into the second bath maintains a nearly constant, unidirectional flow. This behavior mirrors the transformation of an alternating current into a direct current. To quantify this asymmetry, we introduce a thermal choke ratio based on the difference in oscillation amplitudes. Finally, we employ Floquet theory [47–52] to analyze the stationary, time-averaged heat currents at both ends of the two-level system. This approach allows us to investigate the dependence of these stationary heat currents on various parameters.

This paper is structured as follows. In Sec. II, we introduce the driven NESB with noncommutative coupling and calculate the heat currents into each bath in the first subsection. Applying the polaron transformation, we perform the standard procedures to obtain the quantum master equation (QME) [53], and then nontrivially incorporate the full counting statistics to obtain the heat currents into each bath, respectively. In the next subsection, we employ the Floquet theory to explicitly obtain the stationary mean heat currents within the secular approximation. In Sec. III, we define the thermal choke ratio to characterize the asymmetry of the oscillation amplitudes of the currents into each bath, and consider how the stationary currents respond to the variation of different parameters, i.e., driving amplitude, coupling strength, and noncommutative angle. In Sec. IV, we conclude this study and give some outlooks about the control of oscillating heat currents.

II. MODEL AND METHODS

The model consists of a two-level system and two bosonic baths, as illustrated in Fig. 1, whose Hamiltonian can be

written as

$$
\begin{aligned}
H(t) &= H_S(t) + \sum_{\nu=1,2} H_{B,\nu} + H_{I,1} + H_{I,2} \\
&= \frac{\sigma_z}{2}(E_0 \cos \Omega t + \omega_0) + \sum_{j,\nu} \omega_{j,\nu} b_{j,\nu}^\dagger b_{j,\nu} \\
&\quad + \sigma_\theta \sum_j g_{j,1}(b_{j,1}^\dagger + b_{j,1}) + \sigma_z \sum_j g_{j,2}(b_{j,2}^\dagger + b_{j,2}),
\end{aligned}
\tag{1}
$$

where σ_i ($i = x, y, z$) refers to the Pauli matrix. Here, ω_0 denotes the energy splitting of two-level system, which is monochromatically modulated with frequency Ω and amplitude E_0. To simplify notation and calculations, we adopt natural units throughout this work, setting the reduced Planck constant $\hbar$ and the Boltzmann constant k_B to unity, i.e., $\hbar = k_B = 1$. The bosonic operator $b_{j,\nu}^\dagger$ ($b_{j,\nu}$) creates (annihilates) one photon of mode $\omega_{j,\nu}$ in the νth bath, and $g_{j,\nu}$ represents the original coupling strength between the driven system and the νth bath. We have introduced the noncommutative coupling through $\sigma_\theta = \cos \theta \sigma_x + \sin \theta \sigma_z$ [43,44], different from usual NESB model. When $\theta = \pi/2$, this model is exactly solvable. In this article, we mainly consider the case of $\theta = 0$, where the central system is coupled to two bosonic baths through an amplitude damping channel and a dephasing channel, respectively, unless we focus on the effect of noncommutativity represented by θ. Different from the model in Ref. [44], we fix the coupling to the second bath in z direction instead of x direction. Hereafter, we characterize the baths' effect by the spectral density function $I_\nu(\omega) = \pi \sum_j g_{j,\nu}^2 \delta(\omega - \omega_{j,\nu}) = \alpha_\nu \omega^s \omega_c^{1-s} \exp(-\frac{\omega}{\omega_c})$, and we utilize super-Ohmic spectral density via setting $s = 3$. If not explicitly mentioned, we take the cutoff frequency $\omega_c = 1$ in the numerical simulations, and the dimensionless coupling strength $\alpha_1 = \alpha_2 = 0.01$.

A. Time-dependent currents via the Redfield theory

The calculation of the heat current in NESB can be carried out using the full counting statistics [7]. Since we concern the noncommutative system-bath coupling, we need to introduce two auxiliary counting fields to obtain the currents from each bath, respectively. This is different from the time-independent case, where the magnitude of the current from each bath is equal due to energy conservation. The full counting-statistics procedure incorporates the unitary transformation $U_\nu = \exp(-i\chi_\nu \sum_k \frac{\omega_{k,\nu}}{2} b_{k,\nu}^\dagger b_{k,\nu})$, and therefore the original Hamiltonian is transformed into $H[\frac{\chi}{2}](t) = H_S(t) + \sum_{\nu=1,2} H_{B,\nu} + H_{I,1}[\frac{\chi_1}{2}] + H_{I,2}[\frac{\chi_2}{2}]$, where $\chi = (\chi_1, \chi_2)$. To enable the investigation of the strong coupling regime to the second bath, we perform the polaron transformation on the second bath via $P[\frac{\chi_2}{2}] = \sum_j \frac{g_{j,2}}{\omega_{j,2}}(b_{j,2}^\dagger e^{i\frac{\chi_2}{2}\omega_{j,2}} - b_{j,2} e^{-i\frac{\chi_2}{2}\omega_{j,2}})$. This transformation includes the auxiliary counting field of the second bath, which is recovered to the original polaron transformation when we set $\chi_2 = 0$. The final Hamiltonian for

the total system can be rewritten as

$$H'\left[\frac{\chi}{2}\right](t) = e^{\sigma_z P[\frac{\chi_2}{2}]} H\left[\frac{\chi}{2}\right](t) e^{-\sigma_z P[\frac{\chi_2}{2}]}$$

$$= \frac{\sigma_z}{2}(E_0 \cos \Omega t + \omega_0) + \sum_{j,\nu} \omega_{j,\nu} b_{j,\nu}^{\dagger} b_{j,\nu}$$

$$+ S\left[\frac{\chi_2}{2}\right] \sum_{j} g_{j,1}(b_{j,1}^{\dagger} e^{i\frac{\chi_1}{2}\omega_{j,1}} + b_{j,1} e^{-i\frac{\chi_1}{2}\omega_{j,1}})$$

$$\equiv H_0(t) + H_{SB}\left[\frac{\chi}{2}\right], \qquad (2)$$

where $S[\frac{\chi_2}{2}] = \sigma_z \sin\theta + \sigma_x \cos\theta \cosh(2P[\frac{\chi_2}{2}]) + i\sigma_y \cos\theta \sinh(2P[\frac{\chi_2}{2}])$, and $H_0(t)$ is the noninteracting Hamiltonian.

We can now proceed by applying established procedures for deriving the QME as outlined in, e.g., Ref. [53]. Using the Born-Markovian approximation, we obtain the Hamiltonian in the interaction picture

$$H_{SB}^{I}\left[\frac{\chi}{2}\right](t) = U_0^{\dagger}(t) H_{SB}\left[\frac{\chi}{2}\right] U_0(t)$$

$$= S^{I}\left[\frac{\chi_2}{2}\right](t) \sum_{j} g_{j,1}(b_{j,1}^{\dagger} e^{i\omega_{j,1}t} e^{i\frac{\chi_1}{2}\omega_{j,1}} + \text{H.c.}), \qquad (3)$$

where $U_0(t)$ is the evolution operator for the free Hamiltonian $H_0(t)$. For the sake of conciseness, we omit the interaction picture superscript I in what follows. The evolution of the generalized density matrix is

$$\frac{\partial \rho_S(\boldsymbol{\chi}, t)}{\partial t} = -\int_0^{\infty} ds \text{Tr}_B\left[H_{SB}\left[\frac{\chi}{2}\right](t), [H_{SB}\left[\frac{\chi}{2}\right](t-s),\right.$$

$$\left. \times \rho_S(\boldsymbol{\chi}, t) \otimes \rho_B^{eq}]_{\chi}\right]_{\chi}, \qquad (4)$$

where the subscript χ denotes a generalized commutation relation $[A(\chi), B(\chi)]_{\chi} = A(\chi)B(\chi) - B(\chi)A(-\chi)$. After tedious but straightforward calculations, we obtain the final evolution equation for the diagonal elements of the generalized density matrix

$$\frac{\partial}{\partial t}\begin{pmatrix} \rho_S(\boldsymbol{\chi}, t)_{11} \\ \rho_S(\boldsymbol{\chi}, t)_{22} \end{pmatrix} = \begin{pmatrix} A_{11}(t) & A_{12}(\boldsymbol{\chi}, t) \\ A_{21}(\boldsymbol{\chi}, t) & A_{22}(t) \end{pmatrix}\begin{pmatrix} \rho_S(\boldsymbol{\chi}, t)_{11} \\ \rho_S(\boldsymbol{\chi}, t)_{22} \end{pmatrix}, \qquad (5)$$

where the expressions of time-dependent coefficient matrix's elements are shown in Appendix A. This equation is obtained by applying the vectorization technique to Eq. (4). The time-dependent cumulant-generating function is given by the trace of the generalized density matrix $G(\boldsymbol{\chi}, t) \equiv \ln[\text{Tr}_S \rho_S(\boldsymbol{\chi}, t)]$, which gives the heat current with respect to the νth bath $J_{\nu}(t) \equiv (-1)^{\nu} \frac{\partial}{\partial t} \frac{\partial}{\partial \chi_{\nu}} G(\boldsymbol{\chi}, t)|_{\chi_{\nu}=0}$. We set the direction of the heat current positive when it is from the first bath to the second bath, i.e., $J_1(t) > 0$, and $J_2(t) > 0$ when heat leaves the first bath and enters the second one. That is why we add $(-1)^{\nu}$ in the definition of current above.

The results of the above QME are compared to that of HEOM in Fig. 2. Our results demonstrate a significant suppression of the oscillation amplitude in the current flowing into the second bath. Furthermore, the current direction into
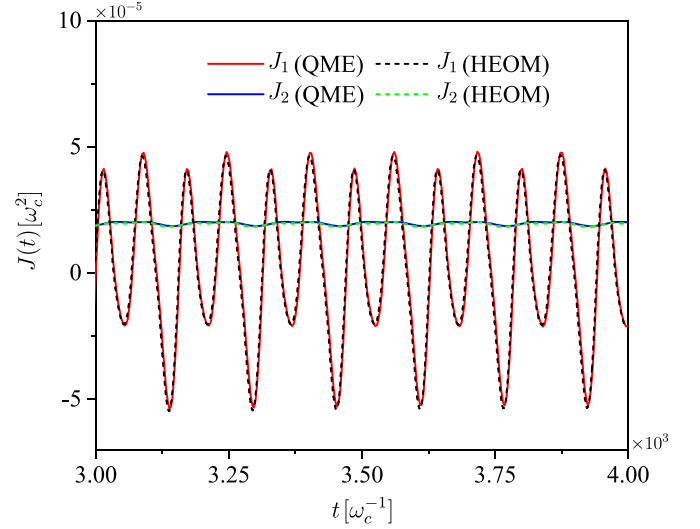

FIG. 2. Heat currents $J_{\nu}(t)$ as a function of time t. The HEOM is utilized with Qutip [54,55], with the maximum depth of the hierarchy being 3 and the cut-off number of exponential terms for approximating the correlation function being 18. We can see that the results of the QME match that of the HEOM well. The noncommutativity $\theta = 0$, and the coupling strengths are $\alpha_1 = \alpha_2 = 0.01$. All variables such as t and $J_{\nu}(t)$ are rescaled with respect to the cutoff frequency ω_c to make the dimensions reasonable hereafter. The sign of the flow represents the direction, e.g., $J_1(t) > 0$ means that the current flows from the first bath into the two-level system, while $J_2(t) > 0$ means that the current flows from the two-level system to the second bath. Obviously, $J_1(t)$ exhibits larger oscillation amplitude compared to $J_2(t)$.

the first bath exhibits periodic reversals, while the current into the second bath maintains a constant direction. This behavior makes the whole system a thermal chokelike device. It makes the oscillation amplitudes of the two-end currents highly asymmetric, thus converting the high-amplitude alternating current into an effectively direct one. Note that the conventional electric choke is usually a two-terminal device while we here consider a more general case that is effectively a three-terminal one [Eq. (1)] incorporating the driving field. The suppression of the oscillation amplitude in the second bath can be attributed to the dephasing channel's limited influence on population change, resulting in a less pronounced current oscillation. Notably, we observe a closer agreement between the results obtained from QME and HEOM for higher temperatures or lower driving frequencies. This convergence stems from the Markovian approximation inherent in the QME approach. As temperature increases, the validity of the Markovian approximation allows for the exploration of higher driving frequencies while still capturing the thermal chokelike behavior. It is important to note that the driving frequency primarily affects the oscillation period of the heat currents, not the occurrence of the thermal choke effect itself.

B. Mean heat currents via the Floquet theory

To gain a deeper physical insight into the dynamics, we investigate the time-independent stationary current via invoking the secular approximation. We carry out this calculation using

the Floquet theory, which makes the secular approximation clearer for the time-dependent Hamiltonian in Eq. (5).

Within the Floquet theory, the Floquet Hamiltonian, Floquet basis, and quasienergy of the system part are required, which can be a computationally demanding task. Fortunately, these quantities are directly accessible in our case. Since the system Hamiltonian is $H_S(t) = \frac{\sigma_z}{2}(E_0 \cos \Omega t + \omega_0)$, the Floquet Hamiltonian is $H_F = \frac{\omega_0}{2}\sigma_z$, whose eigenstates are $|u_{+(-)}(0)\rangle = |\uparrow (\downarrow)\rangle$. The micromotion operator $K(t) = \frac{E_0}{2\Omega}\sin \Omega t \sigma_z$ can be obtained from the evolution operator and the Floquet Hamiltonian, and hence the Floquet basis, is $|u_{+(-)}(t)\rangle = e^{-iK(t)}|u_{+(-)}(0)\rangle = |\uparrow\rangle e^{-i\frac{E_0}{2\Omega}\sin \Omega t}$ $(|\downarrow\rangle e^{i\frac{E_0}{2\Omega}\sin \Omega t})$. Expanding the interaction picture operators in terms of the eigenstates of the Floquet Hamiltonian, we find

$$\langle u_\alpha(0)|\sigma_x(t)|u_\beta(0)\rangle$$

$$= \langle u_\alpha(t)|\sigma_x|u_\beta(t)\rangle e^{i(\epsilon_\alpha - \epsilon_\beta)t}$$

$$= \sum_n \frac{1}{T}\int_0^T dt' [\langle u_\alpha(t')|\sigma_x|u_\beta(t')\rangle e^{-in\Omega t'}]e^{i(\epsilon_\alpha - \epsilon_\beta + n\Omega)t}, \tag{6}$$

where $\epsilon_+ = \frac{\omega_0}{2}, \epsilon_- = -\frac{\omega_0}{2}$ are the eigenvalues of the Floquet Hamiltonian. With the above type of relations, we deal with the expressions like $\sigma_x(t)\sigma_x(t-s)\rho_S(\chi, t)$ frequently encountered in the derivation of QME. In the Floquet theory, we apply the secular approximation (or the rotating-wave approximation) more clearly by eliminating the exponential terms oscillating as a function of time t rather than the variable of integration s. The details are presented in Appendix B. Finally, we get the evolution equation with a constant-coefficient Lindblad superoperator

$$\frac{\partial}{\partial t}\begin{pmatrix}\rho_S(\chi, t)_{11} \\ \rho_S(\chi, t)_{22}\end{pmatrix} = \begin{pmatrix}F_{11} & F_{12}(\chi) \\ F_{21}(\chi) & F_{22}\end{pmatrix}\begin{pmatrix}\rho_S(\chi, t)_{11} \\ \rho_S(\chi, t)_{22}\end{pmatrix}. \tag{7}$$

The stationary solution of the above generalized master equation gives two time-independent heat currents into each bath [31,56], which is the derivative of the eigenvalue with the largest real value of the coefficient matrix with respect to $i\chi_\nu$, i.e.,

$$\bar{J}_\nu = (-1)^{\nu+1}\frac{\frac{\partial F_{12}(\chi)}{\partial(i\chi_\nu)}F_{21}(\chi) + \frac{\partial F_{21}(\chi)}{\partial(i\chi_\nu)}F_{12}(\chi)}{F_{11} + F_{22}}\Bigg|_{\chi=0}. \tag{8}$$

As seen in Fig. 3, they are the same as the time average of the time-dependent currents in the above subsection. To distinguish the mean heat current from the time-oscillating one, we adopt the symbol $\bar{J}$ to denote the time-averaged mean heat current [Eq. (8)] according to the Floquet theory, and $\langle J_\nu \rangle_T$ to represent the numerical average of time-dependent currents obtained from Eq. (5) over a single period.

Note that Eq. (7) differs from Eq. (5) due to the inclusion of the secular approximation in the former. The secular approximation averages out rapidly oscillating terms in the master equation, as given in Eq. (B1). Consequently, the Lindblad-type equations typically lose the information about the oscillatory behavior of the heat currents.
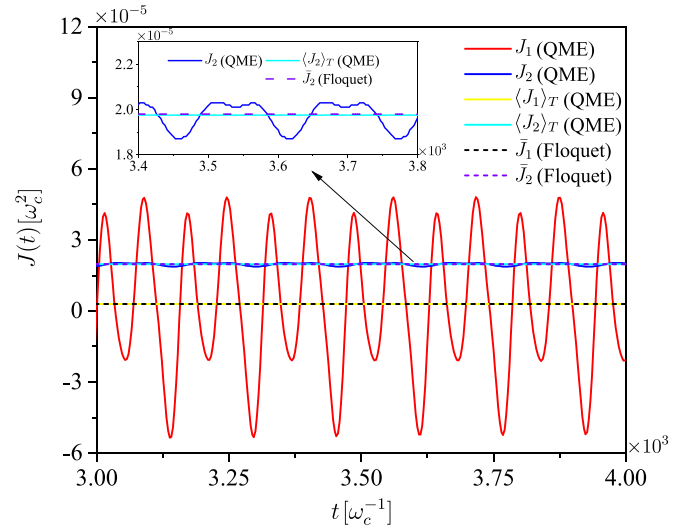

FIG. 3. Comparison between Floquet mean currents $\bar{J}_\nu$, time-dependent oscillating currents $J_\nu(t)$ via QME, and their numerical averages per period $\langle J_\nu \rangle_T$ from each bath. The results demonstrate that $\bar{J}_\nu$ coincides with $\langle J_\nu \rangle_T$. This observation demonstrates that the Lindblad equation, relying on the secular approximation, generally yields time-averaged stationary heat currents. A similar observation is found for the population dynamics, as given in Refs. [57,58].

III. RESULTS AND DISCUSSIONS

A. Thermal choke ratio

The noncommutative coupling in the NESB model gives rise to a thermal chokelike behavior, which can significantly modify the oscillation amplitudes of the currents flowing from or into the baths. This current oscillation can be utilized to perform precise thermal management or reservoir engineering. To characterize the degree of asymmetry of the oscillation amplitudes, we define the normalized thermal choke ratio in terms of the amplitudes of two ends due to noncommutative coupling as

$$\eta := \frac{A_1 - A_2}{\max_\theta\{A_1 - A_2\}}, \tag{9}$$

where A_1 refers to the oscillation amplitude of the current flowing out of the first bath and A_2 to the current flowing into the second bath. Our definition and discussions of the thermal choke ratio go beyond the time-independent rectification ratio and step into the periodically driven thermal analogues of electronic devices. Next, we investigate how the thermal choke ratio changes with the noncommutativity θ in Fig. 4. We observe a monotonic decrease in the thermal choke ratio with increasing θ. This signifies a diminishing asymmetry in the oscillation amplitudes of the currents as the noncommutativity weakens. This behavior is a direct consequence of the quantum nature of noncommutativity. Since the thermal choke ratio is normalized, η is maximum when $\theta = 0$ representing the largest noncommutativity. When $\theta = \frac{\pi}{2}$, the noncommutativity vanishes, and the oscillations of both currents disappear, indicating that the two-level system with two dephasing baths is not a good candidate for heat transport.

Figure 5 demonstrates that increasing the coupling strength α_2 to the second bath can indeed reduce the asymmetry in
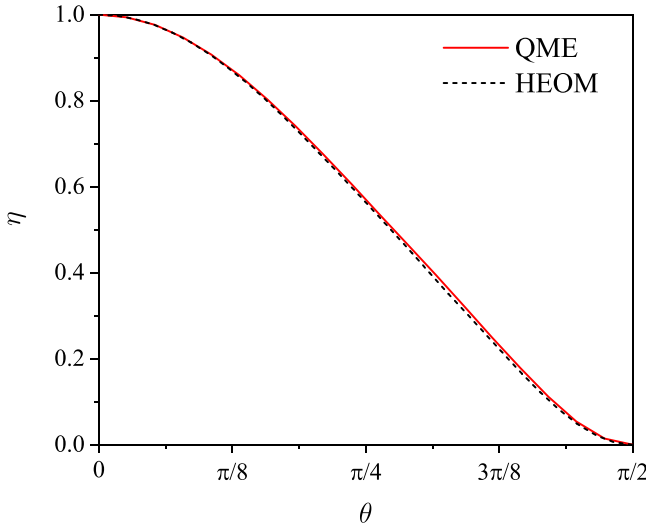
FIG. 4. Thermal choke ratio as a function of the noncommutativity θ.

FIG. 6. (a) Mean heat current $\bar{J}_\nu$ as a function of the driving amplitude E_0. A critical driving amplitude E_c exists where the average heat current vanishes, indicating no net energy injection from the first bath. (b) Mean heat current $\bar{J}_\nu$ as a function of the coupling strength, where $\alpha_1 = \alpha_2 = \alpha$. The average energy flow from the system to the second bath becomes unidirectional, with the heat current oscillating largely from the first bath. Notably, the mean current into the second bath exhibits a power-law dependence, i.e., $\bar{J}_2 \sim \alpha^2$, within the range of small coupling strength.

the oscillation amplitudes of the currents induced by noncommutative coupling. This offers an additional means for fine-tuning the oscillation amplitudes of both currents. However, as the figure reveals, achieving a significant reduction in asymmetry requires a relatively large disparity between the coupling strengths of the two baths. Furthermore, the results in Fig. 5 also highlight the remarkable robustness of the thermal chokelike behavior in our model to variations in coupling strength.

It is important to note that variations in coupling strengths alone, without the introduction of noncommutativity, can also induce an asymmetry in the oscillation amplitudes of the heat currents. However, achieving a significant asymmetry

necessitates an exceedingly large difference between the two coupling strengths. Additionally, excessively weak coupling is required, resulting in a vanishing mean heat current flowing into the corresponding bath. Consequently, even with distinct oscillation amplitudes, the absence of a net unidirectional energy flow disqualifies this approach from being considered a viable thermal choke effect. Conversely, the scheme relying on the noncommutativity exhibits this asymmetry intrinsically, without sacrificing other degrees of freedom.

B. Mean heat current

In this subsection, we investigate the properties of the stationary mean heat current, which are directly related to the average energy transport.

The stationary mean heat currents $\bar{J}_\nu$ from each bath are determined by the Floquet theory, which corresponds to the time average of the oscillating currents $J_\nu(t)$. These mean currents often characterize the long-term behavior of heat transport. In Fig. 6(a), we consider how these stationary heat currents depend to the variation of the driving amplitude E_0. When $E_0 = 0$, the two currents are equal due to energy conservation. The heat current initially flows from the first bath to the two-level system and then into the second bath. However, as the driving amplitude increases, the injected energy alters the flow direction of heat, leading to a reversal of the current back into the first bath. Notably, compared to the significant variation observed in the current from the first bath,
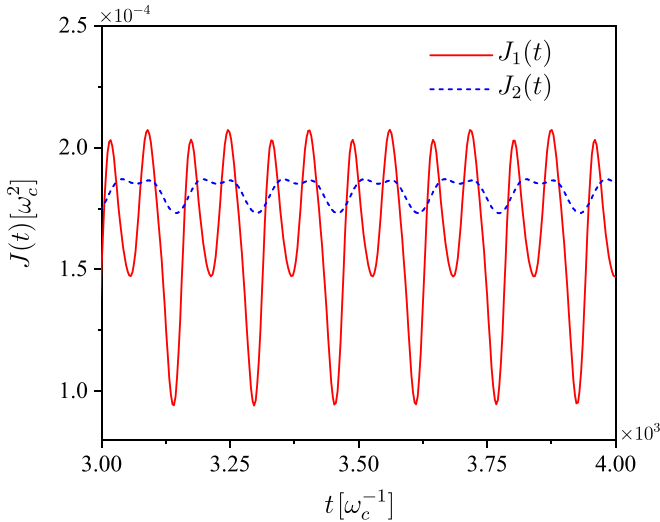

FIG. 5. Compensation of the oscillation amplitude of current via enhancing the coupling strength to the second bath. Here we set the coupling strength as $\alpha_1 = 0.01$, $\alpha_2 = 0.1$ while the other parameters remain the same as that for Fig. 2. Compared with Fig. 2, the oscillation amplitude of the second bath's current becomes larger and comparable with that of the first bath's current.
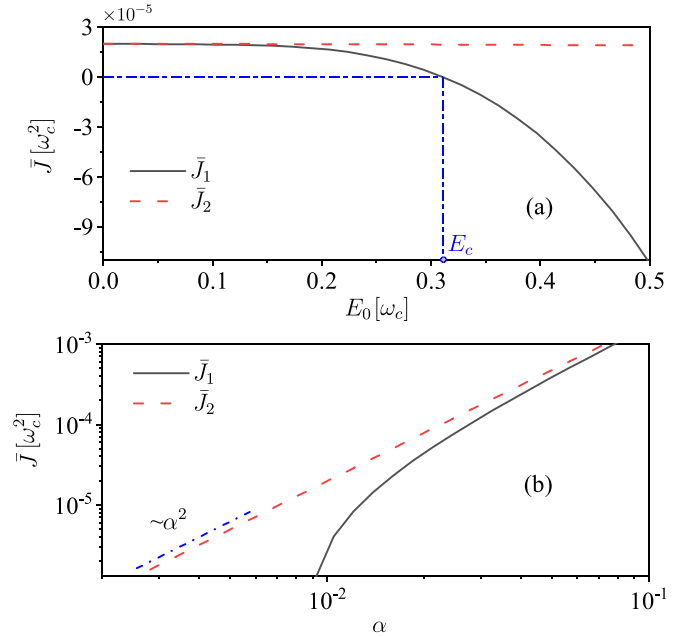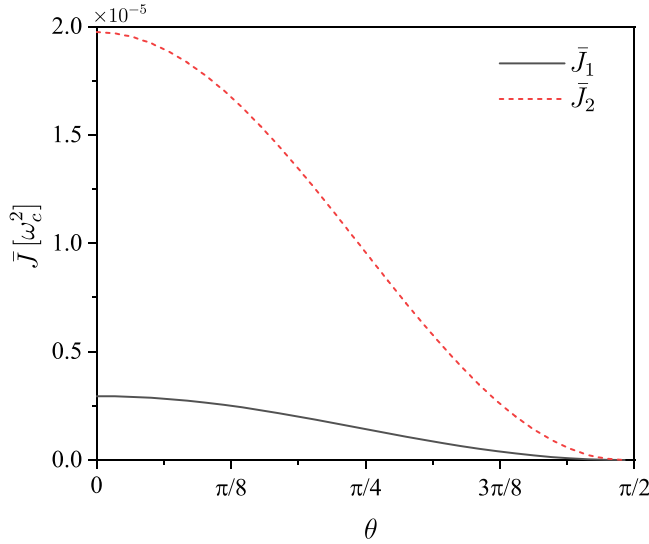
FIG. 7. Mean heat currents $\bar{J}_\nu$ with respect to the noncommutativity θ. One can find that the absolute ratio between the two currents $|J_1/J_2|$ is independent of θ from the Eq. (8).

the current flowing into the second bath remains relatively unaffected. This behavior reflects the decreased sensitivity of the dephasing channel to energy transport. In Fig. 6(b), we observe that the mean current entering the second bath maintains a quadratic dependence on the coupling strength α, as predicted by previous studies [44,59] in no driving case. This is in contrast to the current from the first bath, which exhibits a more complex behavior due to the reversal of its flow direction caused by the driving field. This can be understood from the Lindblad superoperator's elements of Eq. (7). The derivative of $\exp(Q_2)$ (see Appendix B) with respect to $i\chi_2$ gives an additional $\partial Q_2/\partial(i\chi_2)$. Since the functions C_1 and Q_2 are both proportional to the coupling strength α, the expression in Eq. (8) is proportional to α^2.

In Fig. 7, we illustrate the change of the mean currents with respect to the noncommutativity θ. When $\theta = \frac{\pi}{2}$, both currents vanish. Along with the decrease of θ, i.e., the increase of noncommutativity, the magnitudes of both currents ascend. When $\theta = 0$, the mean stationary current entering the second bath exceeds that from the first bath due to a blocking effect

of the injected energy on the current from the first bath. In conclusion, when $\theta = 0$, the current flowing into the second bath exhibits a larger average value and experiences less oscillation.

IV. CONCLUSIONS AND OUTLOOK

In summary, we present a model for achieving quantum thermal choke behavior by employing noncommutative coupling between a system and heat baths. When the direction of the system-bath coupling is the same as that of the modulated energy splitting, the corresponding heat current's oscillation is largely suppressed. This approach facilitates achieving a thermal chokelike effect characterized by a unidirectional heat current on one side of the system, while the current on the opposite side exhibits continuous directional switching. This behavior bears a resemblance to the rectification of alternating electric current into direct current. We further define the thermal choke ratio to characterize the change of current amplitudes. Besides, we illustrate that the secular approximation is the reason why Lindblad-type equations always give the stationary currents even when the system is periodically driven. Our discussions improve the control of heat flow, and hence assist in manipulating the oscillation amplitude of heat currents with more efficiency and precision. Together with previous discussions of the time-averaged heat current, the thermal analog of electronics will find applications in thermal information processing.

For future outlook, the non-Markovian effect [60] on the oscillating heat currents and the discussions of backflow [61] are interesting to investigate. Additionally, having established control over current oscillation amplitudes, future work will explore the generalizability of this model to finite-size heat baths. [62,63].

APPENDIX A: DERIVATION OF THE TIME-DEPENDENT EVOLUTION EQUATION FOR GENERALIZED MASTER EQUATION

We substitute Eq. (3) into the evolution equation of the generalized density matrix Eq. (4), and the first term becomes

$$-\int_0^\infty ds \operatorname{Tr}_B H_{SB}\left[\frac{\boldsymbol{\chi}}{2}\right](t) H_{SB}\left[\frac{\boldsymbol{\chi}}{2}\right](t-s)\left[\rho_S(\boldsymbol{\chi},t) \otimes \rho_B^{eq}\right]$$

$$= -\int_0^\infty ds \operatorname{Tr}_{B1}\left[\sum_j g_{j,1}(b_{j,1}^\dagger e^{i\frac{\chi}{2}\omega_{j,1}} e^{i\omega_{j,1}t} + \text{H.c.}) \sum_j g_{j,1}(b_{j,1}^\dagger e^{i\frac{\chi}{2}\omega_{j,1}} e^{i\omega_{j,1}(t-s)} + \text{H.c.})\rho_{B1}^{eq}\right]$$

$$\times \left\{\operatorname{Tr}_{B2}\left[\cosh\left[\sum_j \frac{2g_{j,2}}{\omega_{j,2}}(b_{j,2}^\dagger e^{i\frac{\chi}{2}\omega_{j,2}} - \text{H.c.})\right] \cosh\left[\sum_j \frac{2g_{j,2}}{\omega_{j,2}}(b_{j,2}^\dagger e^{i\frac{\chi}{2}\omega_{j,2}} e^{-i\omega_{j,2}s} - \text{H.c.})\right]\rho_{B2}^{eq}\right]\right.$$

$$\times \sigma_x(t)\sigma_x(t-s)\rho_S(\boldsymbol{\chi},t)\cos^2\theta$$

$$+ \text{Tr}_{B2}\left[\cosh\left[\sum_j \frac{2g_{j,2}}{\omega_{j,2}}(b_{j,2}^\dagger e^{i\frac{\chi}{2}\omega_{j,2}} - \text{H.c.})\right]\sinh\left[\sum_j \frac{2g_{j,2}}{\omega_{j,2}}(b_{j,2}^\dagger e^{i\frac{\chi}{2}\omega_{j,2}}e^{-i\omega_{j,2}s} - \text{H.c.})\right]\rho_{B2}^{eq}\right]i\sigma_x(t)\sigma_y(t-s)\rho_S(\chi,t)\cos^2\theta$$

$$+ \text{Tr}_{B2}\left[\sinh\left[\sum_j \frac{2g_{j,2}}{\omega_{j,2}}(b_{j,2}^\dagger e^{i\frac{\chi}{2}\omega_{j,2}} - \text{H.c.})\right]\cosh\left[\sum_j \frac{2g_{j,2}}{\omega_{j,2}}(b_{j,2}^\dagger e^{i\frac{\chi}{2}\omega_{j,2}}e^{-i\omega_{j,2}s} - \text{H.c.})\right]\rho_{B2}^{eq}\right]i\sigma_y(t)\sigma_x(t-s)\rho_S(\chi,t)\cos^2\theta$$

$$- \text{Tr}_{B2}\left[\sinh\left[\sum_j \frac{2g_{j,2}}{\omega_{j,2}}(b_{j,2}^\dagger e^{i\frac{\chi}{2}\omega_{j,2}} - \text{H.c.})\right]\sinh\left[\sum_j \frac{2g_{j,2}}{\omega_{j,2}}(b_{j,2}^\dagger e^{i\frac{\chi}{2}\omega_{j,2}}e^{-i\omega_{j,2}s} - \text{H.c.})\right]\rho_{B2}^{eq}\right]\sigma_y(t)\sigma_y(t-s)\rho_S(\chi,t)\cos^2\theta$$

$$+ \text{Tr}_{B2}\left[\cosh\left[\sum_j \frac{2g_{j,2}}{\omega_{j,2}}(b_{j,2}^\dagger e^{i\frac{\chi}{2}\omega_{j,2}}e^{i\omega_{j,2}t} - \text{H.c.})\right]\rho_{B2}^{eq}\right]\sigma_x(t)\sigma_z\rho_S(\chi,t)\sin\theta\cos\theta$$

$$+ \text{Tr}_{B2}\left[\cosh\left[\sum_j \frac{2g_{j,2}}{\omega_{j,2}}(b_{j,2}^\dagger e^{i\frac{\chi}{2}\omega_{j,2}}e^{i\omega_{j,2}(t-s)} - \text{H.c.})\right]\rho_{B2}^{eq}\right]\sigma_z\sigma_x(t-s)\rho_S(\chi,t)\sin\theta\cos\theta + \rho_S(\chi,t)\sin^2\theta\Bigg\}$$

$$= -\int_0^\infty ds C_1(s)\left[\left(\frac{1}{2}\eta e^{-Q_2(s)} + \frac{1}{2}\eta e^{Q_2(s)}\right)\sigma_x(t)\sigma_x(t-s)\rho_S(\chi,t)\cos^2\theta - \left(\frac{1}{2}\eta e^{-Q_2(s)} - \frac{1}{2}\eta e^{Q_2(s)}\right)\right.$$

$$\times\ \sigma_y(t)\sigma_y(t-s)\rho_S(\chi,t)\cos^2\theta$$

$$\left. + \sqrt{\eta}\sigma_x(t)\sigma_z\rho_S(\chi,t)\sin\theta\cos\theta + \sqrt{\eta}\sigma_z\sigma_x(t-s)\rho_S(\chi,t)\sin\theta\cos\theta + \rho_S(\chi,t)\sin^2\theta\right], \tag{A1}$$

where we define $Q_2(t) = \frac{4}{\pi}\int_0^\infty d\omega \frac{I_2(\omega)}{\omega^2}(\frac{1}{e^{\beta\omega}-1}e^{i\omega t} + (\frac{1}{e^{\beta\omega}-1}+1)e^{-i\omega t})$, $\eta_2 = \exp[-Q_2(0)]$, and $C_1(t) = \frac{1}{\pi}\int_0^\infty d\omega I_1(\omega)$ $[\coth\frac{\beta_1\omega}{2}\cos\omega t - i\sin\omega t]$. The other three terms in the expansion of Eq. (4) are calculated in a similar way.

Since the counting of the heat current is only determined by the diagonal elements of generalized density matrix $\rho_S(\chi,t)$, we apply the vectorization on the above four terms and obtain the evolution equation for the diagonal elements of $\rho_S(\chi,t)$:

$$\frac{\partial}{\partial t}\begin{pmatrix}\rho_S(\chi,t)_{11}\\ \rho_S(\chi,t)_{22}\end{pmatrix} = \begin{pmatrix} A_{11}(t) & A_{12}(\chi,t)\\ A_{21}(\chi,t) & A_{22}(t)\end{pmatrix}\begin{pmatrix}\rho_S(\chi,t)_{11}\\ \rho_S(\chi,t)_{22}\end{pmatrix}. \tag{A2}$$

The explicit expressions for the time-dependent coefficient Lindblad superoperator elements are

$$A_{11}(t) = -\int_0^\infty ds C_1(-s)\eta_2\cos^2\theta e^{Q_2(-s)}e^{-i\phi(s,t)} - \int_0^\infty ds C_1(s)\eta_2\cos^2\theta e^{Q_2(s)}e^{i\phi(s,t)} + 4\int_0^\infty ds D_1(s)\sin^2\theta,$$

$$A_{12}(\chi,t) = \int_0^\infty ds C_1(s-\chi_1)\eta_2\cos^2\theta e^{Q_2(-\chi_2+s)}e^{-i\phi(s,t)} + \int_0^\infty ds C_1(-s-\chi_1)\eta_2\cos^2\theta e^{Q_2(-\chi_2-s)}e^{i\phi(s,t)},$$

$$A_{21}(\chi,t) = \int_0^\infty ds C_1(s-\chi_1)\eta_2\cos^2\theta e^{Q_2(-\chi_2+s)}e^{i\phi(s,t)} + \int_0^\infty ds C_1(-s-\chi_1)\eta_2\cos^2\theta e^{Q_2(-\chi_2-s)}e^{-i\phi(s,t)},$$

$$A_{22}(t) = -\int_0^\infty ds C_1(-s)\eta_2\cos^2\theta e^{Q_2(-s)}e^{i\phi(s,t)} - \int_0^\infty ds C_1(s)\eta_2\cos^2\theta e^{Q_2(s)}e^{-i\phi(s,t)} + 4\int_0^\infty ds D_1(s)\sin^2\theta, \tag{A3}$$

where $\phi(s,t) = (\omega_0 s + \frac{E_0}{\Omega}(\sin[\Omega(s-t)] + \sin[\Omega t]))$, and $D_1(s) = -C_1(s) - C_1(-s) + C_1(s-\chi_1) + C_1(-s-\chi_1)$. The presence of time-dependent elements within the Lindblad superoperator renders an analytical solution to the evolution equation intractable. However, the heat current flowing between the system and the baths can be determined numerically using the fourth-order Runge-Kutta method.

APPENDIX B: FLOQUET THEORY FOR THE STATIONARY HEAT CURRENTS

One usually seeks for the stationary heat current rather than the time-dependent one, which is directly related to the average energy. With the Floquet method, which makes the secular approximation more clear, we obtain the stationary heat current. The key point is to address the expressions such as $\sigma_x(t)\sigma_x(t-s)\rho_S(\chi,t)$ and $\sigma_y(t)\sigma_y(t-s)\rho_S(\chi,t)$. We take one matrix element of

$\sigma_x(t)\sigma_x(t-s)\rho_S(\chi, t)$ as an example. Equation (6) in the main text gives

$$\langle\uparrow|\sigma_x(t)\sigma_x(t-s)\rho_S(\boldsymbol{\chi}, t)|\uparrow\rangle = \sum_{n,m}\frac{1}{T^2}\int_0^T e^{-in\Omega t'}e^{i\frac{E_0}{\Omega}\sin\Omega t'}dt'\int_0^T e^{-im\Omega t''}e^{-i\frac{E_0}{\Omega}\sin\Omega t''}dt'' e^{i(\omega_0+n\Omega)t}e^{i(-\omega_0+m\Omega)(t-s)}\rho_S(\boldsymbol{\chi}, t)_{11}$$

$$= \sum_n \mathcal{B}_n\left(\frac{E_0}{\Omega}\right)\mathcal{B}_{-n}\left(-\frac{E_0}{\Omega}\right)e^{i(\omega_0+n\Omega)s}\rho_S(\boldsymbol{\chi}, t)_{11}, \tag{B1}$$

where we only take $m = -n$ in the summation in the last equality and $\mathcal{B}_n$ is the nth Bessel function of the first kind. This is just the secular approximation (or rotating-wave approximation) and is usually justified with relatively large Ω compared to the relaxation time and intrinsic characteristic time of the system. This method yields the constant-coefficient Lindblad superoperator and hence time-independent steady currents.

Applying the above reduction repeatedly, we obtain the following time-independent evolution equation

$$\frac{\partial}{\partial t}\begin{pmatrix}\rho_S(\boldsymbol{\chi}, t)_{11}\\ \rho_S(\boldsymbol{\chi}, t)_{22}\end{pmatrix} = \begin{pmatrix}F_{11} & F_{12}(\boldsymbol{\chi})\\ F_{21}(\boldsymbol{\chi}) & F_{22}\end{pmatrix}\begin{pmatrix}\rho_S(\boldsymbol{\chi}, t)_{11}\\ \rho_S(\boldsymbol{\chi}, t)_{22}\end{pmatrix}, \tag{B2}$$

where the expressions for the coefficient matrix elements are given by

$$F_{11} = 4\int_0^\infty ds D_1(s)\sin^2\theta - \int_0^\infty ds C_1(s)\eta e^{Q_2(s)}\cos^2\theta\sum_n \mathcal{B}_n\left(\frac{E_0}{\Omega}\right)\mathcal{B}_{-n}\left(-\frac{E_0}{\Omega}\right)e^{i(\omega_0+n\Omega)s}$$

$$- \int_0^\infty ds C_1(-s)\eta e^{Q_2(-s)}\cos^2\theta\sum_n \mathcal{B}_n\left(-\frac{E_0}{\Omega}\right)\mathcal{B}_{-n}\left(\frac{E_0}{\Omega}\right)e^{i(-\omega_0+n\Omega)s},$$

$$F_{22} = 4\int_0^\infty ds D_1(s)\sin^2\theta - \int_0^\infty ds C_1(s)\eta e^{Q_2(s)}\cos^2\theta\sum_n \mathcal{B}_n\left(-\frac{E_0}{\Omega}\right)\mathcal{B}_{-n}\left(\frac{E_0}{\Omega}\right)e^{i(-\omega_0+n\Omega)s}$$

$$- \int_0^\infty ds C_1(-s)\eta e^{Q_2(-s)}\cos^2\theta\sum_n \mathcal{B}_n\left(\frac{E_0}{\Omega}\right)\mathcal{B}_{-n}\left(-\frac{E_0}{\Omega}\right)e^{i(\omega_0+n\Omega)s},$$

$$F_{12} = \int_0^\infty ds C_1(-\chi_1 - s)\eta e^{Q_2(-\chi_2-s)}\cos^2\theta\sum_n \mathcal{B}_n\left(\frac{E_0}{\Omega}\right)\mathcal{B}_{-n}\left(-\frac{E_0}{\Omega}\right)e^{i(\omega_0+n\Omega)s}$$

$$+ \int_0^\infty ds C_1(-\chi_1 + s)\eta e^{Q_2(-\chi_2+s)}\cos^2\theta\sum_n \mathcal{B}_n\left(\frac{E_0}{\Omega}\right)\mathcal{B}_{-n}\left(-\frac{E_0}{\Omega}\right)e^{i(-\omega_0-n\Omega)s},$$

$$F_{21} = \int_0^\infty ds C_1(-\chi_1 - s)\eta e^{Q_2(-\chi_2-s)}\cos^2\theta\sum_n \mathcal{B}_n\left(-\frac{E_0}{\Omega}\right)\mathcal{B}_{-n}\left(\frac{E_0}{\Omega}\right)e^{i(-\omega_0+n\Omega)s}$$

$$+ \int_0^\infty ds C_1(-\chi_1 + s)\eta e^{Q_2(-\chi_2+s)}\cos^2\theta\sum_n \mathcal{B}_n\left(-\frac{E_0}{\Omega}\right)\mathcal{B}_{-n}\left(\frac{E_0}{\Omega}\right)e^{i(\omega_0-n\Omega)s}. \tag{B3}$$

[1] Y. Dubi and M. Di Ventra, Colloquium: Heat flow and thermoelectricity in atomic and molecular junctions, Rev. Mod. Phys. **83**, 131 (2011).

[2] N. Li, J. Ren, L. Wang, G. Zhang, P. Hänggi, and B. Li, Colloquium: Phononics: Manipulating heat flow with electronic analogs and beyond, Rev. Mod. Phys. **84**, 1045 (2012).

[3] G. Benenti, G. Casati, K. Saito, and R. S. Whitney, Fundamental aspects of steady-state conversion of heat to work at the nanoscale, Phys. Rep. **694**, 1 (2017).

[4] A. Dhar, Heat transport in low-dimensional systems, Adv. Phys. **57**, 457 (2008).

[5] L. Arrachea, Energy dynamics, heat production and heat–work conversion with qubits: Towards the development of quantum machines, Rep. Prog. Phys. **86**, 036501 (2023).

[6] S. Yang, J. Wang, G. Dai, F. Yang, and J. Huang, Controlling macroscopic heat transfer with thermal metamaterials: Theory, experiment and application, Phys. Rep. **908**, 1 (2021).

[7] H. M. Friedman, B. K. Agarwalla, and D. Segal, Quantum energy exchange and refrigeration: A full-counting statistics approach, New J. Phys. **20**, 083026 (2018).

[8] D. Segal and A. Nitzan, Spin-boson thermal rectifier, Phys. Rev. Lett. **94**, 034301 (2005).

[9] B. Li, L. Wang, and G. Casati, Negative differential thermal resistance and thermal transistor, Appl. Phys. Lett. **88**, 143501 (2006).

[10] D. Segal, Heat flow in nonlinear molecular junctions: Master equation analysis, Phys. Rev. B **73**, 205415 (2006).

[11] N. Gupt, S. Bhattacharyya, B. Das, S. Datta, V. Mukherjee, and A. Ghosh, Floquet quantum thermal transistor, Phys. Rev. E **106**, 024110 (2022).

[12] B. Li, L. Wang, and G. Casati, Thermal diode: Rectification of heat flux, Phys. Rev. Lett. **93**, 184301 (2004).

[13] K. Joulain, J. Drevillon, Y. Ezzahri, and J. Ordonez-Miranda, Quantum thermal transistor, Phys. Rev. Lett. **116**, 200601 (2016).

[14] L. Wang and B. Li, Thermal logic gates: Computation with phonons, Phys. Rev. Lett. **99**, 177208 (2007).

[15] L. Wang and B. Li, Thermal memory: A storage of phononic information, Phys. Rev. Lett. **101**, 267203 (2008).

[16] R. Alicki, D. Gelbwaser-Klimovsky, and G. Kurizki, Periodically driven quantum open systems: Tutorial, arXiv:1205.4552.

[17] K. Szczygielski, D. Gelbwaser-Klimovsky, and R. Alicki, Markovian master equation and thermodynamics of a two-level system in a strong laser field, Phys. Rev. E **87**, 012120 (2013).

[18] X. Cao, C. Wang, and D. He, Driving induced coherent quantum energy transport, Phys. Rev. B **108**, 245401 (2023).

[19] M. Xu, J. Stockburger, G. Kurizki, and J. Ankerhold, Minimal quantum thermal machine in a bandgap environment: Non-markovian features and anti-zeno advantage, New J. Phys. **24**, 035003 (2022).

[20] G. T. Landi, D. Poletti, and G. Schaller, Nonequilibrium boundary-driven quantum systems: Models, methods, and properties, Rev. Mod. Phys. **94**, 045006 (2022).

[21] A. Kopp and K. Le Hur, Universal and measurable entanglement entropy in the spin-boson model, Phys. Rev. Lett. **98**, 220401 (2007).

[22] M. L. Wall, A. Safavi-Naini, and A. M. Rey, Boson-mediated quantum spin simulators in transverse fields: XY model and spin-boson entanglement, Phys. Rev. A **95**, 013602 (2017).

[23] G. Clos and H.-P. Breuer, Quantification of memory effects in the spin-boson model, Phys. Rev. A **86**, 012115 (2012).

[24] L. Nicolin and D. Segal, Non-equilibrium spin-boson model: Counting statistics and the heat exchange fluctuation theorem, J. Chem. Phys. **135**, 164106 (2011).

[25] W. Wu and W.-L. Zhu, Heat transfer in a nonequilibrium spin-boson model: A perturbative approach, Ann. Phys. **418**, 168203 (2020).

[26] W.-M. Zhang, P.-Y. Lo, H.-N. Xiong, M. W.-Y. Tu, and F. Nori, General non-Markovian dynamics of open quantum systems, Phys. Rev. Lett. **109**, 170402 (2012).

[27] H.-P. Breuer, B. Kappler, and F. Petruccione, The time-convolutionless projection operator technique in the quantum theory of dissipation and decoherence, Ann. Phys. **291**, 36 (2001).

[28] A. J. Leggett, S. Chakravarty, A. T. Dorsey, M. P. A. Fisher, A. Garg, and W. Zwerger, Dynamics of the dissipative two-state system, Rev. Mod. Phys. **59**, 1 (1987).

[29] D. Xu and J. Cao, Non-canonical distribution and non-equilibrium transport beyond weak system-bath coupling regime: A polaron transformation approach, Front. Phys. **11**, 110308 (2016).

[30] U. Weiss, *Quantum Dissipative Systems* (World Scientific, Singapore, 2012).

[31] C. Wang, J. Ren, and J. Cao, Nonequilibrium energy transfer at nanoscale: A unified theory from weak to strong coupling, Sci. Rep. **5**, 11787 (2015).

[32] H. Zheng, Dynamics of a two-level system coupled to ohmic bath: A perturbation approach, Eur. Phys. J. B **38**, 559 (2004).

[33] R. Bulla, T. A. Costi, and T. Pruschke, Numerical renormalization group method for quantum impurity systems, Rev. Mod. Phys. **80**, 395 (2008).

[34] N. Makri and D. E. Makarov, Tensor propagator for iterative quantum time evolution of reduced density matrices. I. Theory, J. Chem. Phys. **102**, 4600 (1995).

[35] N. Makri and D. E. Makarov, Tensor propagator for iterative quantum time evolution of reduced density matrices. II. Numerical methodology, J. Chem. Phys. **102**, 4611 (1995).

[36] A. Strathearn, P. Kirton, D. Kilda, J. Keeling, and B. W. Lovett, Efficient non-Markovian quantum dynamics using time-evolving matrix product operators, Nat. Commun. **9**, 3322 (2018).

[37] P. P. Orth, A. Imambekov, and K. Le Hur, Nonperturbative stochastic method for driven spin-boson model, Phys. Rev. B **87**, 014305 (2013).

[38] Y. Tanimura, Numerically "exact" approach to open quantum dynamics: The hierarchical equations of motion (heom), J. Chem. Phys. **153**, 020901 (2020).

[39] Y. Tanimura, Stochastic Liouville, Langevin, Fokker–Planck, and master equation approaches to quantum dissipative systems, J. Phys. Soc. Jpn. **75**, 082001 (2006).

[40] M. M. Wilde, *Quantum Information Theory* (Cambridge University Press, Cambridge, 2013).

[41] P. Menczel, E. Loisa, K. Brandner, and C. Flindt, Thermodynamic uncertainty relations for coherently driven open quantum systems, J. Phys. A **54**, 314002 (2021).

[42] C.-J. Zou, Y. Li, J.-K. Xu, J.-B. You, C. E. Png, and W.-L. Yang, Geometrical bounds on irreversibility in squeezed thermal bath, Entropy **25**, 128 (2023).

[43] D. Gelbwaser-Klimovsky and A. Aspuru-Guzik, Strongly coupled quantum heat machines, J. Phys. Chem. Lett. **6**, 3477 (2015).

[44] C. Duan, C.-Y. Hsieh, J. Liu, J. Wu, and J. Cao, Unusual transport properties with noncommutative system–bath coupling operators, J. Phys. Chem. Lett. **11**, 4080 (2020).

[45] N. Anto-Sztrikacs, F. Ivander, and D. Segal, Quantum thermal transport beyond second order with the reaction coordinate mapping, J. Chem. Phys. **156**, 214107 (2022).

[46] B. Bhandari, P. T. Alonso, F. Taddei, F. von Oppen, R. Fazio, and L. Arrachea, Geometric properties of adiabatic quantum thermal machines, Phys. Rev. B **102**, 155407 (2020).

[47] S. Restrepo, J. Cerrillo, V. M. Bastidas, D. G. Angelakis, and T. Brandes, Driven open quantum systems and Floquet stroboscopic dynamics, Phys. Rev. Lett. **117**, 250401 (2016).

[48] G. Engelhardt, G. Platero, and J. Cao, Discontinuities in driven spin-boson systems due to coherent destruction of tunneling: Breakdown of the Floquet-Gibbs distribution, Phys. Rev. Lett. **123**, 120602 (2019).

[49] G. Engelhardt and J. Cao, Dynamical symmetries and symmetry-protected selection rules in periodically driven quantum systems, Phys. Rev. Lett. **126**, 090601 (2021).

[50] Y. Yan, Z. Lü, and H. Zheng, Resonance fluorescence of strongly driven two-level system coupled to multiple dissipative reservoirs, Ann. Phys. **371**, 159 (2016).

[51] T. Shirai, T. Mori, and S. Miyashita, Condition for emergence of the Floquet-Gibbs state in periodically driven open systems, Phys. Rev. E **91**, 030101(R) (2015).

[52] T. Mori, Floquet states in open quantum systems, Annu. Rev. Condens. Matter Phys. **14**, 35 (2023).

[53] H.-P. Breuer and F. Petruccione, *The Theory of Open Quantum Systems* (Oxford University Press, Oxford, 2007).

[54] J. Johansson, P. Nation, and F. Nori, QuTiP: An open-source Python framework for the dynamics of open quantum systems, Comput. Phys. Commun. **183**, 1760 (2012).

[55] N. Lambert, T. Raheja, S. Cross, P. Menczel, S. Ahmed, A. Pitchford, D. Burgarth, and F. Nori, QuTiP-BoFiN: A bosonic and fermionic numerical hierarchical-equations-of-motion library with applications in light-harvesting, quantum control, and single-molecule electronics, Phys. Rev. Res. **5**, 013181 (2023).

[56] C. Wang, J. Ren, and J. Cao, Unifying quantum heat transfer in a nonequilibrium spin-boson model with full counting statistics, Phys. Rev. A **95**, 023610 (2017).

[57] S.-W. Li, C. Cai, and C. Sun, Steady quantum coherence in non-equilibrium environment, Ann. Phys. **360**, 19 (2015).

[58] Z. Nafari Qaleh and A. T. Rezakhani, Enhancing energy transfer in quantum systems via periodic driving: Floquet master equations, Phys. Rev. A **105**, 012208 (2022).

[59] L.-A. Wu and D. Segal, Quantum heat transfer: A Born-Oppenheimer method, Phys. Rev. E **83**, 051114 (2011).

[60] X. Cao, C. Wang, H. Zheng, and D. He, Quantum thermal transport via a canonically transformed redfield approach, Phys. Rev. B **103**, 075407 (2021).

[61] K. Hashimoto, G. Tatara, and C. Uchiyama, Spin backflow: A non-Markovian effect on spin pumping, Phys. Rev. B **99**, 205304 (2019).

[62] S. V. Moreira, P. Samuelsson, and P. P. Potts, Stochastic thermodynamics of a quantum dot coupled to a finite-size reservoir, Phys. Rev. Lett. **131**, 220405 (2023).

[63] H. Yuan, Y.-H. Ma, and C. P. Sun, Optimizing thermodynamic cycles with two finite-sized reservoirs, Phys. Rev. E **105**, L022101 (2022).